ChemComm

COMMUNICATION

View Article Online
View Journal

Cite this: DOI: 10.1039/c7cc03239k

Received 26th April 2017,
Accepted 16th May 2017

DOI: 10.1039/c7cc03239k

rsc.li/chemcomm

A label-free ratiometric electrochemical DNA sensor for monitoring intracellular redox homeostasis†

Xinping Liu,[ab] Zhengqing Yan,[ac] Yuhuan Sun,[ab] Jinsong Ren[a] and Xiaogang Qu*[a]

A label-free ratiometric electrochemical biosensor was constructed for monitoring intracellular redox homeostasis by DNA metallization-mediated hybridization chain reaction amplification. This platform could also be used to discriminate cancer cells and normal cells.

As a primary modulator of cell microenvironmental reactions, the intracellular redox state plays significant roles in regulating cell behavior and function.[1] The imbalance of intracellular redox homeostasis can affect DNA and RNA synthesis, signal transduction, enzyme activation and even the cell proliferation, and may cause severe diseases, such as cancer and Parkinson's disease.[1,2] Hence, it has garnered considerable research attention to monitor intracellular redox homeostasis over the past decades.

Glutathione (GSH), the most abundant thiol-containing tripeptide in biological systems, is regarded as the key molecule to maintain the intracellular redox homeostasis. The measurement of GSH concentration, therefore, has been used for evaluating the intracellular redox state.[3] To date, several elegant methods, such as colorimetric methods, high-performance liquid chromatographic methods, fluorescence assays and electrochemical techniques, have been reported for the determination of GSH.[4] Compared to other approaches, electrochemical techniques have attracted researchers' particular attention due to the sensitive and rapid response, simple instrumentation and the low cost. With the electro-active nature of GSH, its electrochemical detection *via* direct oxidation has been demonstrated in clinical application. Unfortunately, the direct oxidation of GSH using an electrochemical method is not a fully satisfactory strategy due to the poor voltammetric behavior of GSH.[5] With the bloom of DNA-based assays and nanotechnology, functional biomaterial-based strategies have been widely used for GSH detection. For instance, Lai *et al.* reported an ingenious design and fabrication of a DNA-based electrochemical GSH sensor.[4i] Another promising design was reported by Xu's group.[6] By using manganese dioxide nanosheets, an electrochemiluminescence strategy for detecting GSH was presented.[6] However, false negative or positive errors may occur in these single-signaling electrochemical biosensors because of the presence of many disturbing factors, including indicator concentration, electrode contamination and environmental conditions, especially for a "turn-off" electrochemical biosensor. More recently, a ratiometric method has been employed in electrochemical biosensors.[7] The dual-signal current ratiometry enables the measurement with remarkably enhanced accuracy and sensitivity because an electrochemical ratiometric assay can eliminate intrinsic systematic errors of biosensors. However, so far, it has not been reported to use an electrochemical ratiometric biosensor for monitoring GSH levels. In addition, owing to the ultralow level of GSH under normal physiological conditions, a signal amplification strategy is clearly required for improving both the sensitivity and selectivity of the electrochemical biosensor. To this end, a highly sensitive and label-free approach for monitoring GSH levels based on an electrochemical ratiometric assay and a signal amplification strategy has been constructed in this report.

Thanks to DNA's strong affinity for metal ions, DNA-templated metallization represents a popular approach to fabricate a defined metal nanostructure, which shows promising application in diverse fields.[8] Meanwhile, since the metallization can significantly destroy DNA recognition properties, it can control the hybridization of DNA strands.[9a,b] On the other hand, our and other groups have demonstrated that GSH has a high affinity to several noble metal surfaces, such as silver nanoparticles (AgNPs).[9] Inspired by these interesting and applicable features, for the first time, we developed a label-free ratiometric electrochemical GSH biosensor by DNA metallization-mediated hybridization chain reaction (HCR) amplification. The HCR is a novel enzyme-free amplification method, where target molecules or initiators as triggers lead to the formation of DNA polymers. Two types of hairpin DNA strands (H_1 and H_2) as building blocks can coexist stably in the same system, while the

[a] *Laboratory of Chemical Biology and State Key Laboratory of Rare Earth Resource Utilization, Changchun Institute of Applied Chemistry, Chinese Academy of Sciences, Changchun, Jilin 130022, China. E-mail: xqu@ciac.ac.cn; Fax: +86-431-85262656*

[b] *University of Science and Technology of China, Hefei, Anhui 230029, China*

[c] *University of Chinese Academy of Sciences, Beijing 100039, China*

† Electronic supplementary information (ESI) available: Experimental details, supporting figures. See DOI: 10.1039/c7cc03239k

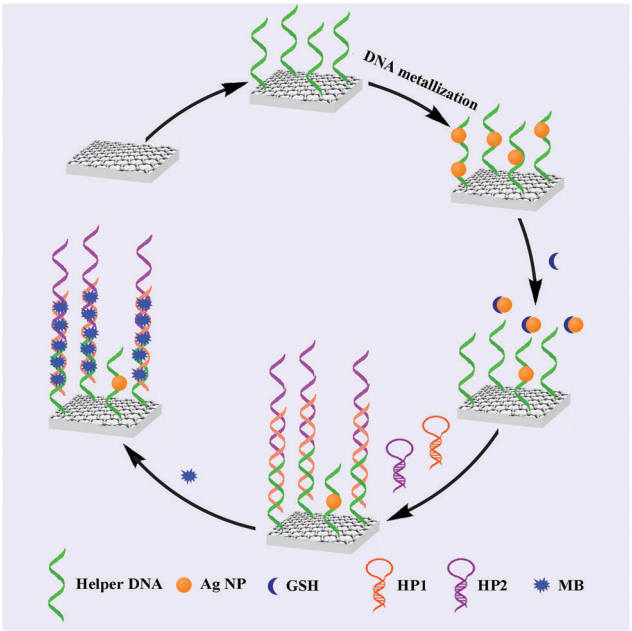

Fig. 1 The illustration of label-free ratiometric electrochemical determination of GSH by DNA metallization-mediated HCR amplification.

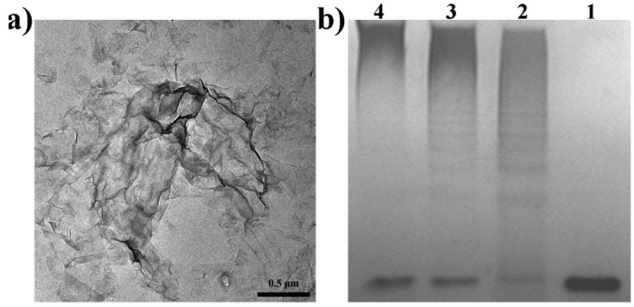

Fig. 2 (a) TEM of TCPP/CCG. (b) The effect of hDNA concentrations on HCR amplification (from right to left: lane 1 : 3 μM H_1 + 3 μM H_2, lane 2 : 3 μM H_1 + 3 μM H_2 + 1.5 μM hDNA, lane 3 : 3 μM H_1 + 3 μM H_2 + 0.6 μM hDNA, lane 4 : 3 μM H_1 + 3 μM H_2 + 0.3 μM hDNA).

presence of helper DNA (hDNA) triggers the occurrence of the hybridization event immediately, which yields a self-assembled double-stranded DNA (dsDNA) nanostructure with numerous repeats.[10] Our strategy is illustrated in Fig. 1. *Meso*-tetra (4-carboxyphenyl) porphine (TCPP), a water-soluble porphyrin, was used to stabilize chemically converted graphene (CCG). The TCPP/CCG modified glassy carbon electrode (GCE) presented more negatively charged carboxyl groups for NH_2-modified hDNA linking and retained the high conductivity of graphene.[11] Meanwhile, ethanolamine was chosen to passivate the unreacted NHS ester.[12] Afterwards, the conjugated hDNA was used as an efficient template for the deposition of AgNPs, which could disturb DNA base pairing and hinder further DNA hybridization. Upon the addition of GSH, the AgNPs would be liberated from hDNA due to the stronger interaction between AgNPs and GSH, which resulted in significant reduction of the peak current of Ag to AgCl (I_{Ag}). Then, the released hDNA further triggered the *in situ* HCR to form self-assembled long DNA fragments. Methylene blue (MB), a widely used electro-active indicator which could intercalate into dsDNA, was used to monitor the HCR process by measuring the "off–on" current (I_{MB}). In this way, GSH could be monitored by recording the ratiometric signal (I_{MB}/I_{Ag}). Taken together, this assay was label-free and facile in operation, avoiding the use of a dye-modified nucleic acid or tedious synthesis. Importantly, the ratiometric biosensor with a self-calibrated characteristic could eliminate the intrinsic systematic error, and the ratiometric output signal I_{MB}/I_{Ag} was increased with HCR amplification. These unprecedented advantages enabled this assay to be highly sensitive and accurate.

The preparation of the electrode material TCPP/CCG was according to a previous report[11] and its corresponding characterization is described in detail in the ESI† (Fig. S1, S2 (ESI†) and Fig. 2a).[11] Before constructing the amplified ratiometric platform for the detection of GSH, it was essential to examine the occurrence of the HCR process triggered by hDNA. We used the gel electrophoresis mobility shift assay to testify. As shown in Fig. 2b, in the absence of hDNA (sequence in Table S1, ESI†), the mixture of H_1 and H_2 did not cause the HCR process owing to the unchanged base number (Fig. 2b, lane 1). Upon exposure to hDNA, as indicated in Fig. 2b, lanes 2–4, the prolonged DNA product was observed. This demonstrated the occurrence of the HCR process. In addition, it was found that the average length of the formed DNA nanostructure was inversely related to the amount of hDNA (Fig. 2b, lanes 2–4), which suggested that a higher concentration of hDNA could induce the increased consumption of H_1 and H_2.[10]

To confirm the utility of this amplified ratiometric platform, we used differential pulse voltammetry (DPV) to characterize MB/HCR/Ag + hDNA/TCPP/CCG (**1**), MB/GSH/Ag + hDNA/TCPP/CCG (**2**) and MB/HCR/GSH/Ag + hDNA/TCPP/CCG (**3**), respectively. The MB probe was chosen in our system because its oxidation potential was fully separated from that of Ag to AgCl. As shown in Fig. 3, (**3**) showed a strong MB signal at about −0.29 V and a weak Ag signal at about +0.15 V *vs.* Ag/AgCl, while (**1**) exhibited a weak MB signal and a strong Ag signal, indicating that the strong interaction between GSH and AgNPs led to the release of hDNA and further triggered the occurrence of the HCR process. Meanwhile, (**3**) presented a significantly stronger MB signal compared to that of (**2**) on account of the HCR amplification effect, demonstrating that I_{MB}/I_{Ag} was increased with HCR amplification. These results indicated the feasibility of the amplified ratiometric biosensor for GSH.

Electrochemical impedance spectroscopy (EIS) is a useful tool for characterizing the modification of an electrode surface and evaluating the sensitivity of an electrochemical biosensor. Using EIS, each step in the fabrication process of the amplified ratiometric biosensor could be readily determined by monitoring the changes of the electron transfer resistance (R_{et}).

The R_{et} value of bare GCE was about 91 Ω. The value increased to 102 Ω with TCPP/CCG assembled on the electrode surface while the R_{et} value increased to 378 Ω for the GO-functionalized electrode surface (Fig. S3, ESI†), indicating the excellent conductivity properties of TCPP/CCG in comparison with GO. As shown in Fig. S4 (ESI†), after the connection of

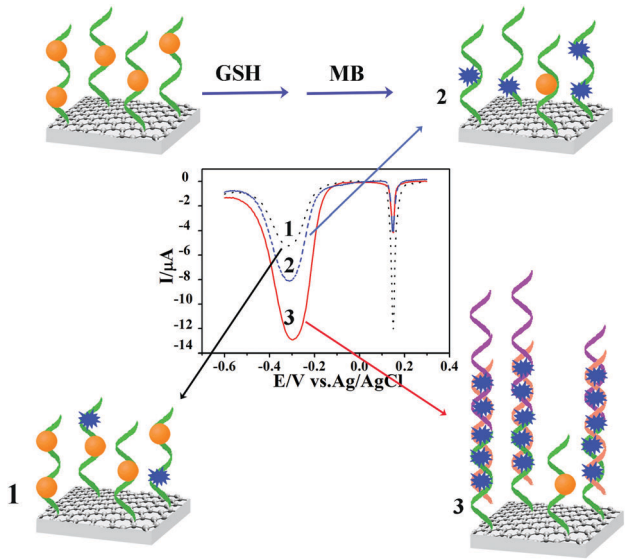

Fig. 3 DPV characterizations of MB/HCR/Ag + hDNA/TCPP/CCG (without GSH) modified GCE (**1**), MB/GSH/Ag + hDNA/TCPP/CCG (without HCR) modified GCE (**2**), and MB/HCR/GSH/Ag + hDNA/TCPP/CCG modified GCE (**3**).

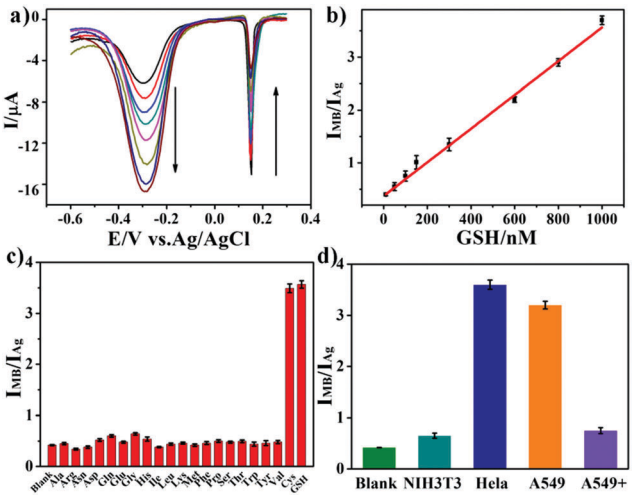

Fig. 4 (a) DPV signals for the amplified ratiometric biosensor in response to different concentrations of GSH. (b) The linear plot. Error bars were estimated from at least three independent measurements. (c) The ratio I_{MB}/I_{Ag} of the probe in the presence of different amino acids. The concentrations of amino acids were 1000 nM. (d) Comparison among different cell extracts: A549, NMM-treated A549 (A549+), HeLa and NIH3T3 cells.

hDNA to the TCPP/CCG modified electrode, the R_{et} value was about 467 Ω. Upon the formation of AgNPs, a remarkable attenuation of R_{et} was observed since hDNA-templated metallization tremendously enhanced the conductive ability of DNA. The concentration of $AgNO_3$ had been optimized (Fig. S5, ESI†). Meanwhile, TEM in Fig. S6 (ESI†) further supported the formation of AgNPs on the hDNA template. Then the addition of GSH in turn increased the R_{et} value because of the demetallization of hDNA. After that, the occurrence of the HCR process further led to an increase of the impedance since negatively charged DNA would repel the redox indicator $[Fe(CN)_6]^{3-/4-}$ close to the GCE surface.

For the evaluation of the analytical performance of the amplified ratiometric biosensor, the changes of I_{MB}/I_{Ag} were immediately recorded with the increase of GSH concentration. The peak current signal of MB was increased with increasing GSH, whereas the peak current signal of Ag to AgCl was gradually decreased (Fig. 4a). The calibration plots displayed a good linear relationship between the ratio I_{MB}/I_{Ag} and the concentration of GSH in the range of 10–1000 nM with the square of correlation coefficient (R^2) at 0.9968 (Fig. 4b). The detection limit of the amplified ratiometric biosensor was down to 103 pM at 3σ (S/N = 3), which was comparable to other reported techniques for detecting GSH (Table S2, ESI†), while a linear relationship between I_{Ag} and the concentration of GSH in the range from 10 nM to 200 nM was obtained. By comparison with the non-ratiometric sensor, the ratiometric GSH sensor exhibited a wider linear range with a comparable detection limit (Fig. S7, ESI†). Meanwhile, the amplified ratiometric biosensor also exhibited ultrahigh selectivity for GSH by recording the values of I_{MB}/I_{Ag} in the presence of different amino acids. The results in Fig. 4c indicated that the ratiometric biosensor had a nearly negligible response to other amino acids except cysteine and GSH, which was mainly ascribed to the high binding affinity between thiol and AgNPs *via* the formation of the Ag–S bond. To further demonstrate the superiority of this ratiometric sensor, we compared the reproducibility of the ratiometric strategy with the non-ratiometric method. Using I_{Ag} and I_{MB}/I_{Ag} values for the quantification of GSH, five parallel measurements were performed on five individual functionalized electrode surfaces. The testing results of I_{Ag} in these measurements greatly varied with a large average standard deviation (SD), while the variation in the response signal was significantly reduced by using I_{MB}/I_{Ag} to indicate the testing results (Fig. S8, ESI†), showing that the ratiometric measurement could cancel out the variation of electrodes and other systematic errors. In addition, a comparison of the analytical performance of the electrochemical ratiometric method with that of a commercial GSH kit is needed. The principle of the commercial GSH kit is based on the cascade reactions mediated by a GSH-specific enzyme and the assay readout is recorded at 412 nm. As presented in Fig. S9 (ESI†), the calibration plots displayed an excellent linear relationship between the absorbance of 412 nm and the concentration of GSH in the range from 1 μM to 50 μM with the square of correlation coefficient (R^2) at 0.9987. And the detection limit of the standard method was 0.7 μM at 3σ (S/N = 3). Then the same sample (5 μM GSH) was detected using both methods. The results were 5.22 μM (electrochemical ratiometric method) and 4.96 μM (GSH kit assay), respectively, confirming the reliability of our electrochemical ratiometric method. Compared with the GSH kit, our approach has advantages in terms of operation and sensitivity. The GSH kit requires complicated procedures and can be compromised due to enzyme inactivity, and the detection limit of the commercial kit for the GSH assay (0.7 μM) is much higher than that of the electrochemical ratiometric method (103 pM).

Since the amplified ratiometric platform possessed excellent selectivity and high sensitivity to GSH, we further extended our

work to determine the intracellular level of GSH. Since cytoplasm possessed a much higher concentration of GSH than those of cysteine and other biothiols, the presence of cysteine and other biothiols would not interfere with GSH biosensing.[4d] The MTT results (Fig. S10, ESI†) revealed that the TCPP/CCG composite had a good biocompatibility and was suited to further biomedical applications. In the following work, we evaluated the GSH levels of two cancer cell lines (A549 and HeLa) and one normal cell line (NIH3T3) by measuring their I_{MB}/I_{Ag}. The ratio signals I_{MB}/I_{Ag} of the prepared biosensor were increased significantly upon incubating with the A549 cell extract, and the calculation result showed that the concentration of GSH in A549 cells was 13.3 mM according to the curve in Fig. 4b, which was in accordance with the previous work.[3] Meanwhile, as illustrated in Fig. 4d, it was found that the I_{MB}/I_{Ag} values were greatly increased upon mixing with the cancer cell (A549 and HeLa) extracts, while it exhibited a nearly negligible response after incubating with the normal cell (NIH3T3) extract. So the prepared biosensor could not only determine GSH in cell extracts but also discriminate between cancer and normal cells. In addition, a previous report indicated that *N*-methylmaleimide (NMM) was a GSH scavenger.[4g] We compared NMM-treated and untreated A549 cell extracts, the results indicated that the ratio value I_{MB}/I_{Ag} of the NMM-treated A549 cell (A549+) was much lower than that of the untreated A549 cell. In addition, intracellular GSH levels were also validated using the commercial GSH kit. The result revealed that the overall GSH level in cancer cells was higher than that of normal cells (Fig. S11, ESI†) and the GSH concentration of A549 cells was 10.9 mM. These results showed the potential of our amplified ratiometric biosensor for clinical determination of GSH.

In summary, the GSH concentration has been used for evaluating intracellular redox homeostasis. We constructed a label-free ratiometric electrochemical DNA sensor for monitoring GSH by DNA metallization-mediated HCR amplification. In the presence of GSH, strong interactions between GSH and AgNPs can result in the release of hDNA, and further trigger the occurrence of the HCR process. This will decrease the Ag signal and increase the MB signal. The amplified ratiometric platform has several advantages. Firstly, the method is simple and label-free. The whole process avoids the use of dye-labelled nucleic acid or tedious synthesis. Secondly, the introduction of the ratiometric assay can cancel out intrinsic systematic errors, and eliminate the likelihood of false negative or positive errors. Thirdly, the ratio signal I_{MB}/I_{Ag} is increased with HCR amplification, enabling the assay to be more sensitive. Furthermore, the amplified ratiometric biosensor can discriminate cancer and normal cells due to their different GSH levels. To our knowledge, this is the first example of using an electrochemical ratiometric DNA sensor for monitoring GSH levels.

This work was supported by 973 Project (2012CB720602) and NSFC (21210002, 21431007, and 21533008).

Notes and references

1 F. Q. Schafer and G. R. Buettner, *Free Radical Biol. Med.*, 2001, **30**, 1191–1212.
2 S. C. Lu, *Mol. Aspects Med.*, 2009, **30**, 42–59.
3 Y. Liu, Y. Tian, Y. Tian, Y. Wang and W. Yang, *Adv. Mater.*, 2015, **27**, 7156–7160.
4 (*a*) X. Chen, Y. Zhou, X. Peng and J. Yoon, *Chem. Soc. Rev.*, 2010, **39**, 2120–2135; (*b*) A. Niazov-Elkan, E. Golub, E. Sharon, D. Balogh and I. Willner, *Small*, 2014, **10**, 2883–2891; (*c*) P. K. Sudeep, S. T. S. Joseph and K. G. Thomas, *J. Am. Chem. Soc.*, 2005, **127**, 6516–6517; (*d*) Y. Xianyu, Y. Xie, N. Wang, Z. Wang and X. Jiang, *Small*, 2015, **11**, 5510–5514; (*e*) Y. Guo, H. Wang, Y. Sun and B. Qu, *Chem. Commun.*, 2012, **48**, 3221–3223; (*f*) Y. Xiao, L. Zeng, T. Xia, Z. Wu and Z. Liu, *Angew. Chem., Int. Ed.*, 2015, **54**, 5323–5327; (*g*) R. Deng, X. Xie, M. Vendrell, Y.-T. Chang and X. Liu, *J. Am. Chem. Soc.*, 2011, **133**, 20168–20171; (*h*) W. Wang, L. Li, S. Liu, C. Ma and S. Zhang, *J. Am. Chem. Soc.*, 2008, **130**, 10846–10847; (*i*) H. R. L. Z. Zhad and R. Y. Lai, *Chem. Commun.*, 2014, **50**, 8385–8387; (*j*) L.-Y. Niu, Y.-S. Guan, Y.-Z. Chen, L.-Z. Wu, C.-H. Tung and Q.-Z. Yang, *J. Am. Chem. Soc.*, 2012, **134**, 18928–18931; (*k*) Y. Luo, L. Zhang, W. Liu, Y. Yu and Y. Tian, *Angew. Chem., Int. Ed.*, 2015, **54**, 14053–14056; (*l*) F. Cao, E. Ju, C. Liu, F. Pu, J. Ren and X. Qu, *Chem. Commun.*, 2016, **52**, 5167–5170; (*m*) J. Ge, Z.-M. Huang, Q. Xi, R.-Q. Yu, J.-H. Jiang and X. Chu, *Chem. Commun.*, 2014, **50**, 11879–11882.
5 J. C. Harfield, C. Batchelor-McAuley and R. G. Compton, *Analyst*, 2012, **137**, 2285–2296.
6 W. Gao, Z. Liu, L. Qi, J. Lai, S. A. Kitte and G. Xu, *Anal. Chem.*, 2016, **88**, 7654–7659.
7 (*a*) L. Wu, X. Zhang, W. Liu, E. Xiong and J. Chen, *Anal. Chem.*, 2013, **85**, 8397–8402; (*b*) Q. Hao, X. Shan, J. Lei, Y. Zang, Q. Yang and H. Ju, *Chem. Sci.*, 2016, **7**, 774–780; (*c*) L. Wu, H. W. Ji, H. J. Sun, C. Ding, J. Ren and X. Qu, *Chem. Commun.*, 2016, **52**, 12080–12083; (*d*) W.-J. Shen, Y. Zhuo, Y.-Q. Chai and R. Yuan, *Anal. Chem.*, 2015, **87**, 11345–11352; (*e*) Y. Du, B. J. Lim, B. L. Li, Y. S. Jiang, J. L. Sessler and A. D. Ellington, *Anal. Chem.*, 2014, **86**, 8010–8016.
8 (*a*) L. Berti, A. Alessandrini and P. Facci, *J. Am. Chem. Soc.*, 2005, **127**, 11216–11217; (*b*) E. Braun, Y. Eichen, U. Sivan and G. Ben-Yoseph, *Nature*, 1998, **391**, 775–778; (*c*) C. F. Monson and A. T. Woolley, *Nano Lett.*, 2003, **3**, 359–363.
9 (*a*) Z. Chen, Y. Lin, C. Zhao, J. Ren and X. Qu, *Chem. Commun.*, 2012, **48**, 11428–11430; (*b*) Y. Lin, Y. Tao, F. Pu, J. Ren and X. Qu, *Adv. Funct. Mater.*, 2011, **21**, 4565–4572; (*c*) B. Hu, Y. Zhao, H.-Z. Zhu and S.-H. Yu, *ACS Nano*, 2011, **4**, 3166–3171; (*d*) C. A. Merkin, R. L. Letsinger, R. C Mucic and J. J. Storhoff, *Nature*, 1996, **382**, 607–609; (*e*) W. Gan, B. Xu and H.-L. Dai, *Angew. Chem., Int. Ed.*, 2011, **50**, 6622–6625; (*f*) J. C. Love, L. A. Estroff, J. K. Kriebel, R. G. Nuzzo and G. M. Whitesides, *Chem. Rev.*, 2005, **105**, 1103–1169.
10 (*a*) R. M. Dirks and N. A. Pierce, *Proc. Natl. Acad. Sci. U. S. A.*, 2004, **101**, 15275–15278; (*b*) J. Huang, Y. Wu, Y. Chen, Z. Zhu, X. Yang, C. J. Yang, K. Wang and W. Tan, *Angew. Chem., Int. Ed.*, 2011, **50**, 401–404.
11 L. Feng, L. Wu, J. Wang, J. Ren, D. Miyoshi, N. Sugimoto and X. Qu, *Adv. Mater.*, 2012, **24**, 125–131.
12 Z. Zhang, L. Wu, J. Wang, J. Ren and X. Qu, *Chem. Commun.*, 2013, **49**, 9986–9988.

